Orientation of Cellulose Nanocrystals Controlled in Perpendicular Directions by Combined Shear Flow and Ultrasound Waves Studied by Small-Angle X-ray Scattering

Frédéric Pignon, Enrico F Semeraro, William Chèvremont, Hugues Bodiguel, Nicolas Hengl, Mohamed Karrouch, Michael Sztucki

Orientation of cellulose nanocrystals controlled in perpendicular directions by combined shear flow and ultrasound waves studied by SAXS

Frédéric Pignon[†], Enrico F. Semeraro[‡], William Chèvremont[†], Hugues Bodiguel[†], Nicolas Hengl[†], Mohamed Karrouch[†], Michael Sztucki[§]*

[†]Univ. Grenoble Alpes, CNRS, Grenoble INP (Institute of Engineering Univ. Grenoble Alpes), LRP, F-38000 Grenoble, France

[‡]University of Graz, Institute of Molecular Biosciences, NAWI Graz, A-8010 Graz, Austria / BioTechMed Graz, A-8010 Graz, Austria

[§]ESRF, The European Synchrotron, CS 40220, F-38043 Grenoble Cedex 9, France

KEYWORDS: Liquid Crystal, cellulose nanocrystal, ultrasound, acoustic radiation, shear flow, SAXS, orientation, structural organization.

ABSTRACT. The combined effect of shear flow and ultrasound (US) waves on the dynamical structural orientations of cellulosic cholesteric liquid crystal were investigated by time-resolved, in situ small-angle X-ray scattering (SAXS). A dedicated channel-type shear-flow/ultrasound cell for SAXS characterization was developed to simultaneously generate a shear-flow-induced horizontal stress force and a US-induced vertical acoustic radiation force. The control of the

alignment of anisometric cellulose nanocrystals (CNCs), with their director parallel to the ultrasonic wave direction of propagation, was revealed at an unprecedented nanometer scale. Concurrently, the application of shear flow induced a horizontal orientation of CNCs with their directors aligned along the velocity direction. By adjusting the level of simultaneously-applied shear flow and US intensity to the CNC suspensions, it was possible to tune the direction and level of orientation of the CNCs during time. For a specific ratio of applied shear rate to acoustic power, some transient orientation of the CNCs at an intermediate angle between horizontal and vertical direction was evidenced. Relaxation of these orientations' phenomena upon cessation of flow and/or US were also highlighted.

INTRODUCTION. Among the most important properties of liquid crystals are their anisometric components (molecules or particles) as well as their specific inter-particle interactions. These features allow liquid crystals to flow easily and, at the same time, to behave as solid crystals because of the macroscopic anisotropic properties induced by the mutual arrangements of their components. In lyotropic liquid crystals made of rod-shaped colloids with a well-defined axis of symmetry, particles are able to align in a preferential common direction with both an orientational order extended on long-range scale and a well-defined positional interparticle distance. The self-assembling characteristics of liquid crystals, combined with their orientational and positional properties, lead to the existence of different kind of phases in the phase diagram. Isotropic, nematic or cholesteric phases can form depending on the particle concentration and interparticle interactions, which in turn are tuned by the chemical composition of the colloidal surface as well as by the physico-chemical properties of the suspending fluid. The fluidity of liquid crystals is also important, as it easily allows the control of different kinds of orientational order and organization phases by external fields that confer anisotropic optical, mechanical or

physical macroscopic properties, and enables the development of advanced materials. Among different external fields (like magnetic or electric fields, known to control the orientation of these liquid crystal phases) the effect of ultrasound, and its orienting action on nematic liquid crystals, was theoretically predicted,[1,2] and experimentally studied.[3-6]

Cellulose nanocrystals (CNCs) are well known systems adopting different liquid crystal phases as isotropic, nematic or cholesteric phases. The structural organization of CNC suspensions at rest and their phase diagram have been well characterized in the literature.[7-16] At rest, CNC suspensions are known to exhibit a phase separation behavior with coexisting isotropic and liquid-crystalline cholesteric phases. Before complete phase separation, the cholesteric phase exists as microdomains, or tactoids, in the isotropic phase.[17-22] The chiral nematic, or cholesteric phase, is characterized by a long-range orientational order of the CNCs combined with a helical modulation of their director (local alignment).[12,23] The phase diagram is characterized by two critical concentrations, C_i, and C_a. Below C_i, the suspension is fully isotropic and above C_a it is fully anisotropic (cholesteric). The coexistence region lies between these two values. Thanks to the specific self-assembly properties of CNCs and the several structural organizations available by many different processes, liquid-crystalline, nano-structured, bio-based composites can be developed.[12,24-28] Such materials can exhibit specific optical properties (iridescence), reinforced mechanical properties (stiffness, anti-crack propagation), or gas-barrier properties. They could then represent high added-value materials in numerous applications such as microelectronics (pressure sensitive screens, photovoltaics),[23,29] tissue engineering (stratified multilayered cartilage, three dimensional porous constructs),[30] or in packaging for bio- and agro- industries.[31] One important challenge for reaching these specific functional properties is to control the orientation and organization of the materials in a wide spatial scale and with controlled external

fields with the best possible efficiency. The parameters that regulate the three different phases of the CNCs (isotropic, nematic and cholesteric) are linked to inter-particle interactions between the nanocrystals as well as to external forces applied to the suspension. Inter-particle interaction can be modified by changing the ionic strength in the suspension medium as well as the surface properties of the nanocrystals (see, e.g., adsorption or grafting processes).[15,32-35] The external forces applied in CNCs suspensions can also change the liquid crystal organization from one phase to another, or cause the mixing of the three phases. The effect of several external solicitations on the CNC structural organizations have been extensively studied in the literature. This includes shear flow field,[9-10,36-44] magnetic field,[45,49] electric field,[29] surface tension in drying processes,[19,20,50,51] and pressure forces in membrane separation processes.[52-54] More specifically, the effect of shear flow on the structural organization of CNCs have been extensively explored from a fundamental[9,10,36-41-44,51,54-56] to an industrial point of view in several processes inducing a flow.[12,19,20,26,27,30,57-62] Ultrasound waves during cross-flow ultrafiltration processes were applied and revealed an alteration of the structural organization of CNCs within the concentrated layers deposited near the membrane surface.[52] More recently, the effects of ultrasound vibration were investigated in another kind of nematic liquid crystals, with induced changes in both molecular orientation and refractive index.[63] Briefly, thanks to a lens structure consisting of a liquid crystal layer, sandwiched between two glass substrates with a piezoelectric ring, Shimizu and coworkers reported changes in the molecular orientation of the liquid crystals, which were induced by ultrasonic resonance flexural vibrations at tens-of-kHz. This device was used to develop a variable focus lens controlled by the input voltage delivered to the piezoelectric ring.[63] However, to the best of our knowledge, no specific study on the US-induced structural orientation of liquid-crystal-like CNC suspensions (as well as induced by the combined

effect of shear flow and US radiation) have been reported and performed at nanometer length scales.

The focus of this work is to study by in situ time-resolved SAXS the combined effect of shear flow and ultrasound waves on the dynamical orientation and structural organization of cellulosic cholesteric liquid crystal suspensions. The structural organization of CNC suspensions studied in this work was already characterized in the past. The suspension is composed of isotropically distributed CNCs (isotropic phase) in coexistence with the volume fraction of liquid crystalline phase, ϕ_{LC} (anisotropic phase).[15,44,54] Dedicated SAXS Shear flow/US-Cell was implemented at the European Synchrotron Radiation Facility (ID02 TRUSAXS beamline) to simultaneously apply a horizontal stress force induced by shear flow and a vertical acoustic radiation force induced by US waves. The results proved that the vertical acoustic radiation force permits to control the alignment of the liquid crystal organization of CNCs along the ultrasonic wave direction of propagation, and that this orientation competes with the shear induced one.

MATERIALS AND METHODS. Cellulose Nanocrystals CNCs were purchased from UMaine Development Center (University of Maine, Orono, ME) as an aqueous suspension with a stock concentration of C = 12.2 wt%. Three different concentrations were prepared by dilution in deionized water and 0.01 mol L^{-1} NaCl, followed by 2 h of vigorous stirring of the suspensions. These suspensions were then sonicated using a sonication probe (Branson Digital sonifier, Marshall Scientific, Hampton, NH), power output of 250 W). A volume of 250 ml of suspensions under agitation with a magnetic stirrer was sonicated applying duty cycle 30 % and output control of 0.5 W. This gives rise to 67.5 W delivered to the sample within 10 minutes. The morphology of the CNCs considered in this work and their phase diagram in aqueous

suspension have been studied in detail in previous publications. SAXS data from diluted suspensions at rest, assuming a parallelepipedal shape for the sonicated CNCs, gave 121 × 20 × 5 nm^3 average dimensions.[15,44,54]

Shear flow/US-Cell. A Shear flow/US-Cell composed of a parallelepipedic channel containing an immersed vibrating blade was developed to, on one hand, apply shear flow and/or ultrasonic waves to the feed suspensions and, on the other hand, to monitor in situ the dynamical structural organization changes by SAXS.[52,64] This cell is made of transparent polycarbonate with a parallelepipedic channel of width H = 4 mm along x, depth W = 7.4 mm along z and length L = 100 mm along y. A titanium vibrating blade of width 3 mm and length 100 mm is immersed and sealed from the upper part of the channel. To apply an acoustic radiation force along z (vertical direction), this blade is connected to a sonotrode (Sodeva TDS, Méry, France) consisting of a piezoelectric transducer attached to a metal rod, which generates ultrasonic waves at a frequency of f_{US} = 20 kHz and at an applied amplitude of a_{US}.[52,64] This amplitude has been measured to a_{US} =1.6 µm thanks to a vibrometry system consisting in a sensor head (OFV 353, Polytec, Waldbronn, Germany), a velocity decoder (OFV3001, Polytec) and an oscilloscope (DPO 3014, Tektronix, Beaverton, OR). For all the measurements presented in this work, only one acoustic radiation force has been applied with an acoustic amplitude of a_{US} =1.6 µm. This corresponds to an acoustic pressure $P = 2\pi\rho c f_{US} a_{US} \cong 297$ kPa and to an acoustic power $P_a = P^2/\rho c \cong 6$ $W.cm^{-2}$, where ρ = 1000 $kg.m^3$ is the water density and c = 1480 $m.s^{-1}$ is the speed of sound in water.

To apply a stress force along y (horizontal) induced by shear flow, the cell was coupled with a syringe pump (PHD 4400, Harvard Apparatus, Cambridge, MA) to vary the flow rate Q and thus the shear rate inside the channel. The flowing circuit was designed in order to be able to push or

pull out the suspension from the syringe through the Shear flow/US-Cell and toward another sealed tank. This allowed to explore different shear flow and US conditions with the same suspension thorough successive separated steps. The influence of the velocity direction that was applied during push (+V) or pull out (-V) steps was also evaluated. In addition, two pressure gauge sensors were connected near the inlet and outlet of the channel to measure the variation of pressures inside the channel during the flow. It enabled to check the achievement of the equilibrium steady state value of applied shear flow for each condition.

Small-Angle X-ray Scattering (SAXS). SAXS measurements were performed at the TRUSAXS ID02 beamline (ESRF, Grenoble).[65] Measurements were performed at room temperature with a sample-detector distance of 10 m and an X-ray wavelength $\lambda = 0.1$ nm, covering a range of scattering vector magnitude, q, of (0.007−0.7) nm^{-1}, where $q = (4\pi/\lambda) \sin(\theta/2)$ with θ the scattering angle. The corresponding nominal lengthscale ($\sim 2\pi/q$) range is 9 nm $\leq l \leq$ 898 nm. Thanks to the pinhole collimation setup available at ID02, all the measurements were acquired by using a beam cross-section at the sample position of about 80 μm vertically and 150 μm horizontally. The incident beam passed through the sample in the Shear flow/US-Cell and the two-dimensional scattered intensity patterns were recorded on a high-resolution CCD detector (MX170, RayoniX, Evanston, IL) (Figure 1). During the experiments, the X-ray beam was directed along the x-direction perpendicular to the walls of the flow cell, through windows of 3 mm × 5.5 mm × 0.3 mm (width × height × thickness) opened into the wall and positioned in middle of the channel ($y = 50$ mm, $z = 3.5$ mm). The cell was mounted in a motorized stage, which allowed to probe the structural organization of the suspension at different distances in both y and z directions. Absolute intensity scale of the scattered intensity [$I(q)$] was deduced from azimuthally averaging of the scattering patterns, after

applying standard detector corrections and normalization. Before the shear flow-US experiments with CNC suspensions, the cell was filled with demineralized water and the normalized background scattering of the cell was firstly registered. This background scattering of the cell filled with water was systematically subtracted to the scattering of the CNC suspensions for all experiments. From the 2D patterns, the analysis of the anisotropy was performed by using the MATLAB-based Small-Angle Scattering Evaluation Tool (SASET) software.[66] Specifically, the model-free Principal Component Analysis (*PCA*) method was chosen, which provides values from 0 (for isotropic suspensions) to 1 (in the case of completely aligned systems), and, depending on the system, is quantitatively comparable to the commonly used order parameter.[66] In the case of aligned, flat beidellite clay-particles, for example, PCA anisotropy values had a logarithmic relationship with the Maier-Saupe width-parameter.[54,66] The anisotropy and direction of maximum scattering (ψ_0) were calculated via *PCA* in the (0.073 – 0.500) nm^{-1} q-range. Annular averages were calculated over this q-vector range to define the scattering intensity as a function of the ψ azimuthal scattering angle in the plane of the 2D SAXS patterns. The application of several shear rates, in both presence and absence of ultrasound waves, allowed to emphasize the relative effect of these two forces on the degree of anisotropy (*PCA anisotropy*) and orientation [maximum scattering direction (ψ_0)] of the CNC suspensions.

RESULTS AND DISCUSSIONS. Three CNC concentrations were studied in the Shear flow/US-Cell via SAXS (Figure 1): the first concentration C = 5.2 wt% (ϕ_{LC} = 0 vol%) is in the isotropic domain while the two others are at the beginning of the biphasic domain C = 7.3 wt% ($\phi_{LC} \approx$ 5 vol%) and C = 9.1 wt% ($\phi_{LC} \approx$ 25 vol%). These concentrations values were evaluated by calculating the mean interparticle distance $d=2\pi/q_{peak}$ between the elementary CNCs, where q_{peak}

is the position of the maximum of $I(q)$. The power law describing the trend of $d(C)$ as a function of C for the same batch of CNC suspensions is described elsewhere[15,54] (Figure S1). Different procedures were used to monitor the time-dependent structural organization of these CNC suspensions: first, the effect of US or shear flow alone, and, second, the combined effect of shear flow and US. The relaxation of the orientations upon cessation of US or shear flow were also studied.

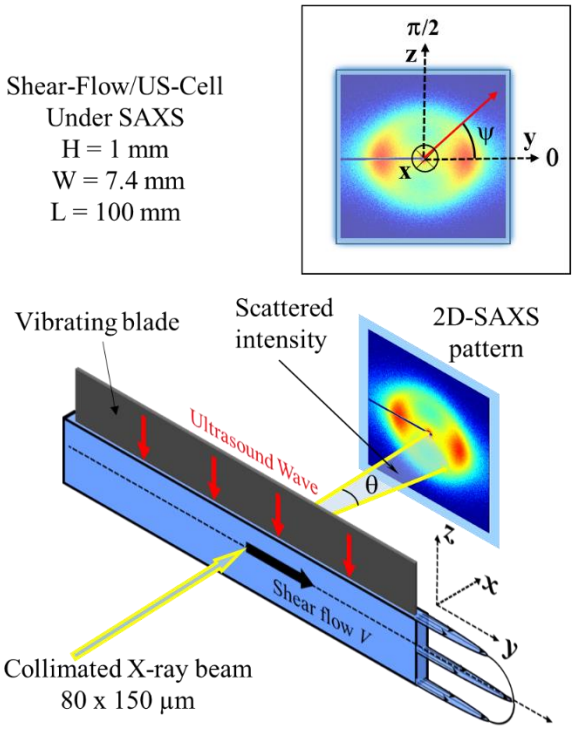

Figure 1. Schematic description of the SAXS experiment with the dedicated Shear flow/US-Cell used to monitor the time dependent changes of structural organization under simultaneously applied shear flow (horizontal stress force) and ultrasound waves (vertical acoustic radiation force).

Effect of US alone on the orientation of CNCs and subsequent relaxation phenomena. The effect of US on CNC liquid crystals was studied by applying a vertical acoustic pressure $P \cong 297$ kPa (corresponding to an acoustic power $P_a \cong 6$ W.cm^{-2}) to a 9.1 wt% CNC suspension at rest in the Shear flow/US-Cell. The evolutions of the 2D-SAXS patterns were monitored under this ultrasound solicitation. As displayed in Figure 2, a few seconds after the start of the sollicitation, we observed an anisotropic pattern, with two peaks in the horizontal direction. It revealed an orientation of the CNCs with their director aligned in the vertical z-direction corresponding to the US radiation propagation. After cessation of the ultrasonic solicitation, the systems relaxed and the pattern evolves slowly towards an isotropic one. In order to describe more quantitatively this phenomenon, we performed systematically a Principal Component Analysis[66] of the anisotropy (*PCA anisotropy*) and determined the maximum scattering direction ψ_0. The *PCA anisotropy* increases sharply from low values corresponding to isotropic SAXS patterns towards a state of about 0.25, which instead corresponds to a well oriented SAXS pattern elongated in the horizontal direction as confirmed by the value of $\psi_0 \cong 180°$. This enhancement of the scattering intensity in the horizontal *y*-direction is attributed to the alignment of the cellulose nanocrystals with their director along the vertical *z*-direction. This is due to the reinforcement of fluctuations in particle concentration in the *y-axis* generated by the regular alignment of the CNCs along *z*. The time dependent increase of *PCA anisotropy* was fitted by a stretched exponential growth, suggesting a complex structural re-orientation involving several mechanisms. This complexity could be associated to the acoustic pressure effect needed to firstly disrupt the cholesteric organization of the CNCs initially existing at rest, and then to induce the orientation of the isolated CNCs until reaching a parallel arrangement in a stable nematic organization.

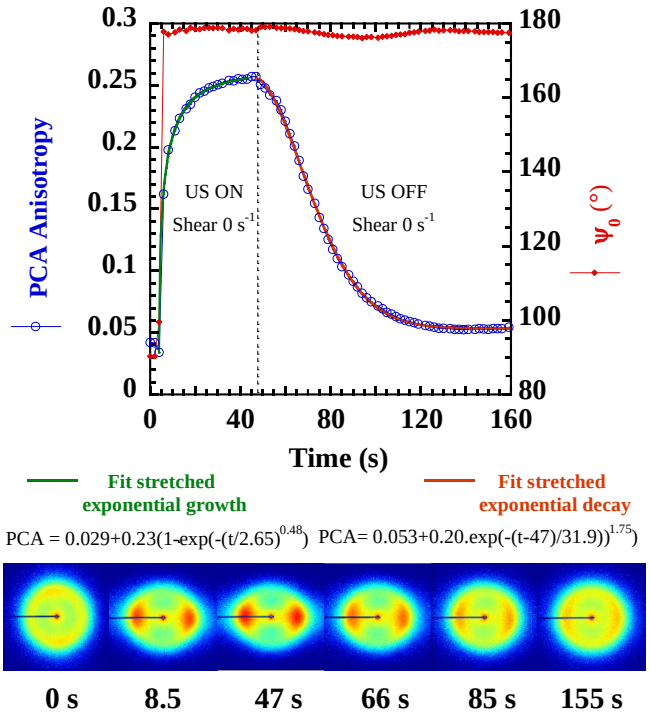

Figure 2. Transient state of orientation level (*PCA anisotropy*) and maximum scattering direction (ψ_0) and corresponding 2D-SAXS patterns of CNC suspensions undergoing vertical acoustic radiation force induced by US at time t = 0 s and then relaxation upon cessation of US at time t = 47 s. C = 9.1 wt%, 0.01 mol L^{-1} NaCl.

From this oriented state, the cessation of US radiation, showed a slower mechanism of relaxation of the orientations, until a stabilization at a lower *PCA anisotropy* value of about 0.05 was reached at about 120 s. The value of $\psi_0 \cong 180°$, suggest that some nematic domains remained aligned along the vertical direction. This relaxation period is needed for the CNCs to recover their initial isotropic organization. Here again a stretched exponential decay fit of the *PCA anisotropy* values could be associated to a relaxation involving several mechanisms: probably firstly a loss of orientation of the isolated CNCs followed by the onset of the local reorganization of CNCs in cholesteric tactoids. In a previous work on the same CNC system and same

concentration,[44] the PCA Anisotropy value at high shear flow of 1000 s^{-1} was about 0.45, which is higher than the one reached in this work under US (0.25). For comparison an equivalent *PCA Anisotropy* value of about 0.25 (the one achieved under US) was reached under flow at shear rate of 5 s^{-1},[44] which gives the order of magnitude of an equivalent shear rate induced by US, if one consider US radiation as a streaming phenomena.[4,5] After a high shear flow of 1000 s^{-1} and upon the cessation of this high shear that induced a complete dissociation of the CNCs, it was evidenced a kinetic of relaxation up to 700 s.[44] In this case, the relaxation time corresponded to a decrease of the *PCA anisotropy* at nanometer scale (calculated from 2D SAXS patterns), and a simultaneous increase in viscosity. At the micrometer scale [probed by small-angle light scattering (SALS)], a corresponding induction time of about 675 s was necessary to reveal the appearance of a pitch and the first re-formation of cholesteric tactoids.[44] In the present work, under US the relaxation time to recover an equilibrium at a low *PCA anisotropy* value close to the one at rest before applying US radiation, seems to be faster, as the *PCA anisotropy* equilibrates to its initial value at about t = 120 s. Consequently, one can infer that the breakdown effect induced by the US radiation on the CNC suspensions would be less destructive than the one induced by a high shear flow. Probably some tactoids will not been completely dissociated under US radiation, which could explain the faster relaxation time under US radiation than the one under high shear flow. Nevertheless, a supplementary study at higher, micrometer length scales would be necessary to confirm this hypothesis.

Effect of shear flow alone followed by US alone on orientation of the CNCs. Assuming a Poiseuille flow, the mean shear rate $\dot{\gamma}_{yx}$ in the rectangular channel was calculated using the following equation:[67]

$$\dot{\gamma}_{yx} = \frac{6Q}{WH^2} \qquad \textbf{(Eq. 1)}$$

Due to non-Newtonian behavior (such as, e.g., shear-thinning behavior highlighted on the CNC suspensions),[15,44] the shear rate can slightly change along the *x* direction (thickness *H* of the channel). In order to evaluate this possible variation of shear rate along the X-ray beam propagation, the apparent shear rate $\dot{\gamma}_a$ of a rectangular die and the wall shear rate $\dot{\gamma}_w$ were calculated (Figure S2).[67] This latter took into account the shear-thinning behavior and corresponding shear-thinning exponent, *n,* for each regimes of flow of CNC suspensions. The values of *n* were deduced from our previous results.[15] One can see that for shear rates belonging to the studied domain the differences are negligible for the three calculated shear rates ($\dot{\gamma}_{yx}$, $\dot{\gamma}_a$, $\dot{\gamma}_w$), therefore confirming the use of Equation 1 to define the different effective, applied shear rates. Q values ranged from 1 mL min^{-1} up to 110 mL min^{-1}, corresponding to $\dot{\gamma}_{yx}$ ranges from 0.8 s^{-1} to 92.9 s^{-1}.

The effect of shear flow on CNC liquid crystals was studied by applying Q = 110 mL min^{-1} from the syringe through the Shear flow/US-Cell, reaching a shear rate $\dot{\gamma}_{yx}$ of 92.9 s^{-1}. In a first step, the suspension was first pushed and then pulled out from the syringe allowing to impose the shear flow in the two velocity directions (+V) or (-V), respectively. The time evolutions of the 2D-SAXS patterns were registered and the corresponding *PCA anisotropy* and ψ_0 were calculated. Under the effect of shear flow, as previously observed,[44] the velocity field induced the orientation of the CNCs with their director aligned in the horizontal direction corresponding to the velocity direction (Figure 3). The *PCA anisotropy* increases sharply from low value of about 0.03 (isotropic SAXS pattern) towards a stable value of about 0.32, corresponding to a well oriented SAXS pattern elongated in the vertical direction, with $\psi_0 \cong 90°$. The simultaneous measurement of the pressure gauge confirmed that the steady state regime was reached in each direction of shear during four successive changes in velocity directions at different shear rates

(Figures S3, S4 and S5). It is interesting to notice that the increase of *PCA anisotropy* from the rest state to the oriented steady state is reached quicker under the effect of this high value of $\dot{\gamma}_{yx}$ = 92.9 s^{-1} (equilibration time of about 7 s) than upon the effect of US radiation (equilibration time of about 30 s). Indeed, this high shear rate belongs to the third regime of the well-known three-regime rheological behavior of these CNC suspensions. It corresponds to the second shear-thinning behavior associated to a fast, complete breakdown of the smaller units of tactoids (in a few seconds) towards the parallel flowing of all nanocrystals along the velocity direction (nematic-like arrangement).[44] In a second step, at time t = 70 s, from this well-orientated state induced by shear flow, US were immediately applied upon cessation of shear flow to the CNC suspension and the corresponding changes in orientation were probed during time. The vertical acoustic pressure induced a flip of the 2D-SAXS pattern elongated from vertical to horizontal direction (change in ψ_0 value from ≅ 90° to ≅ 180°), which corresponds to a flip of the CNC directors aligned along horizontal y to vertical z-direction, respectively. The transient time that was needed to flip the orientation from horizontal to vertical and to reach an equilibrium towards ψ_0 ≅ 180° was about 20 s. This equilibration time is very similar to the one observed in the case the system is initially at rest (see Figure 2), and quicker than the delay of 30 s obtained in the case of cessation of US irradiation. These results allowed to highlight the ability of this tailored set-up to easily tune the liquid crystal CNC orientations and therefore control the succession of perpendicular orientations during time.

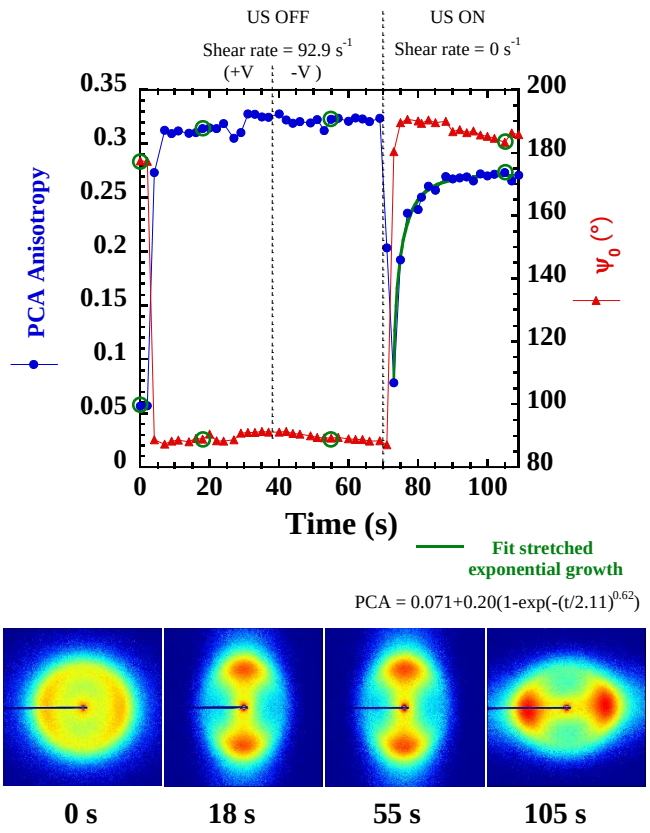

Figure 3. Transient state of orientation level (*PCA anisotropy*) and maximum scattering direction (ψ_0) and corresponding 2D-SAXS patterns of CNC's suspensions firstly submitted to horizontal shear flow along two successive velocity directions (+V) and (-V) and secondly submitted to a vertical acoustic radiation force induced by US radiation upon cessation of flow at time t = 70 s. C = 9.1 wt%, 0.01 mol L^{-1} NaCl.

Time dependent mechanisms of combined effect of US and shear flow. In the aim to evaluate the combined effect of the vertical acoustic radiation force induced by US and of shear, a similar procedure with four steps was implemented. In step 1, only shear was applied (shear ON, US OFF); in step 2 the US radiation was activated together with the same shear rate as step 1 (shear ON, US ON); in step 3 the shear was stopped while the US irradiation was still active (shear OFF, US ON); and finally, in the step 4, also US irradiation was stopped (shear OFF, US OFF).

When applied, the US acoustic pressure was fixed at $P \cong 297$ kPa and several shear rates were explored. From all the measurements explored, some interesting specific competition between shear flow forces and US radiations forces have been emphasized, mostly in a regime of low shear rates. Figure 4, as an example, presents the plots of *PCA anisotropy* and ψ_0 values, along with the corresponding 2D-SAXS patterns for CNC suspensions at $C = 9.1$ wt % and $\dot{\gamma}_{yx} = 2.53$ s^{-1}.

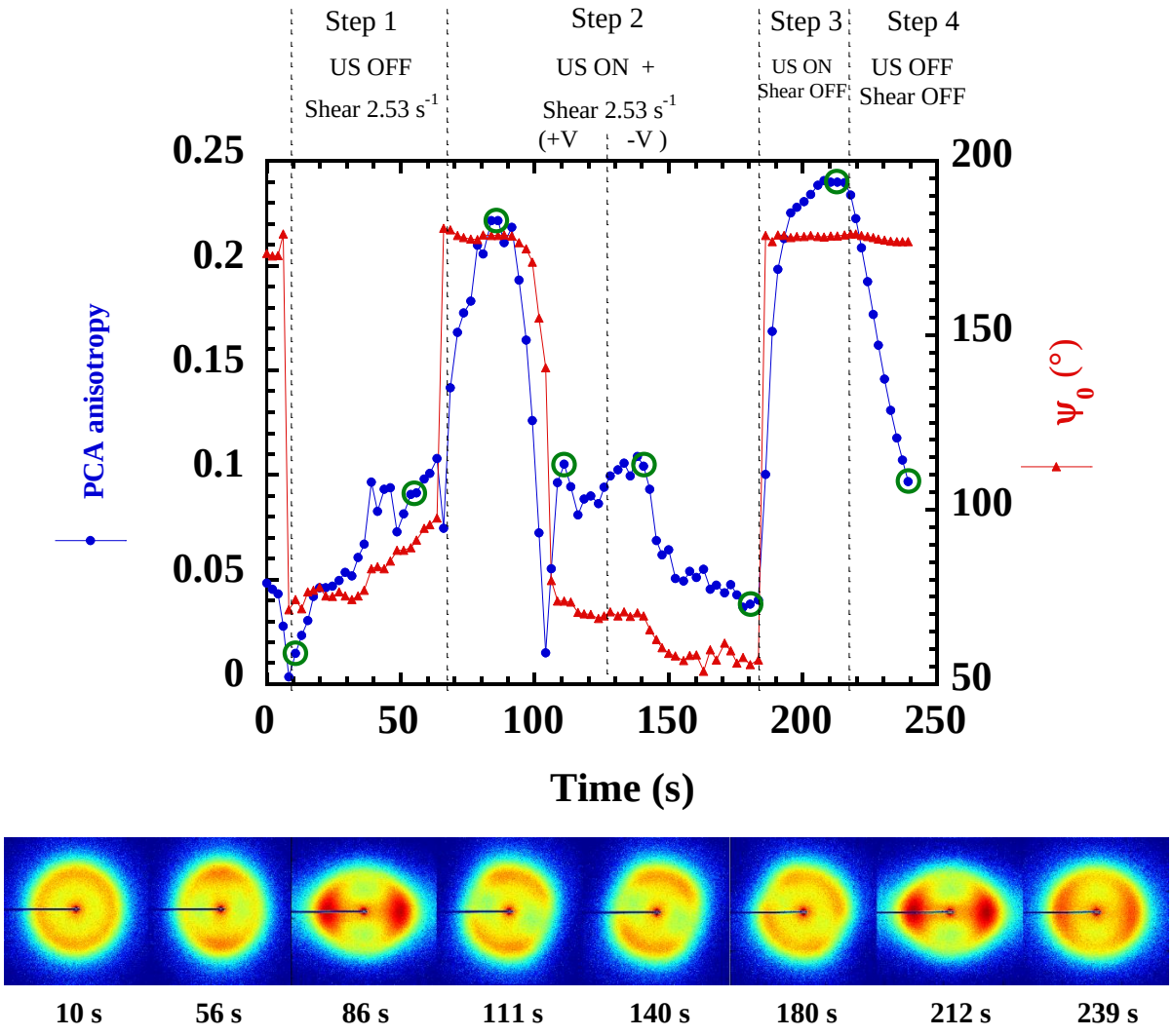

Figure 4. Transient state of orientation level (*PCA anisotropy*) and maximum scattering direction (ψ_0), and corresponding 2D-SAXS patterns of CNC suspensions successively

undergoing step 1: shear flow alone; step 2: shear flow [along two successive velocity directions (+V) and (-V)] associated to US radiation; step 3: US radiation alone; and step 4: no external solicitation. Shear rate applied was $\dot{\gamma}_{yx}$ = 2.53 s^{-1} and acoustic pressure applied was *P* ≅ 297 kPa. *C* = 9.1 wt%, 0.01 mol L^{-1} NaCl.

During step 1, the orientation of CNCs was dominated by the effect of shear and ψ_0 raised towards ≅90°. In step 2, when US radiation was applied, at first, the US radiation dominated the effect of shear (ψ_0 ≅180°). However, at about *t* = 100 s the effect of shear and of US radiation started to equilibrate and the average orientation of the CNCs' director flips towards intermediate values corresponding to ψ_0 of about 60 to 70°, and then keep this range of ψ_0 value between the two solicitations until the end of step 2. In step 3, when shear was stopped, the US radiation alone orients back the CNCs' director along the vertical *z*-direction with ψ_0 ≅180°. Finally, in step 4, after the cessation of US radiation, the CNC orientations and *PCA anisotropy* relaxed towards a lower oriented state. To go further in this time dependent analysis, in step 3 an evolution of the organization during time was observed while constant external fields in shear flow combined with US radiation were simultaneously applied. These results highlight the competition between these two solicitations and their capacity to orient the CNC directors in an intermediate orientation angle between horizontal and vertical directions, which depend on the application history of these two solicitations. For example, the application of US under shear could favor the orientation induced by shear forces as well as re-orientation upon inversion of shear flow direction, which gave rise to unstable orientations during time as shown in Fig. 4

In order to study in more details the relative effect of US radiation and shear, and to highlight the competition between the two, several shear rates conditions under same US radiation level were

explored with the same procedure and time duration for each step. Three different behaviors were evidenced as displayed in (Figure 5).

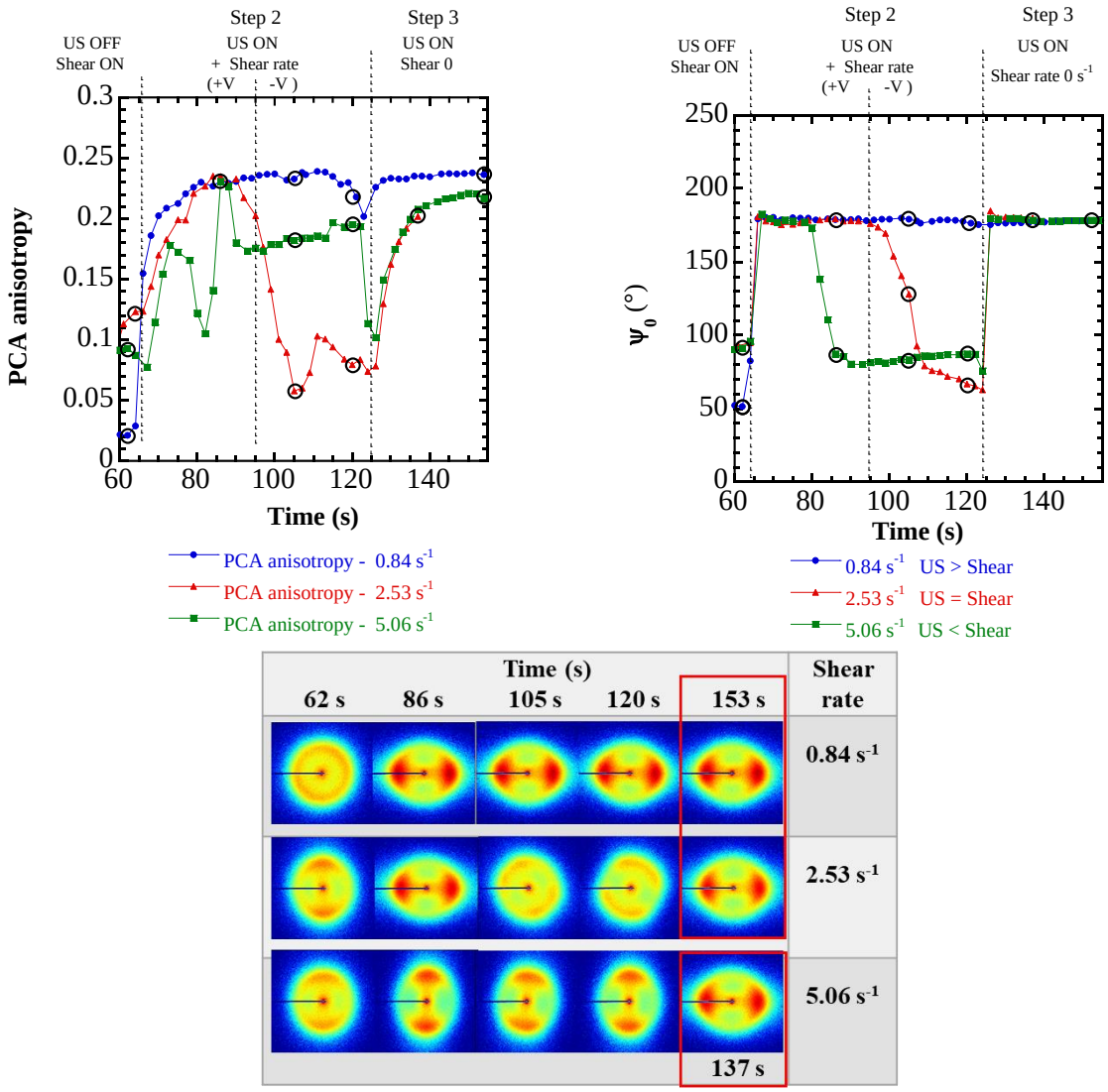

Figure 5. Time dependent mechanisms on orientation level (*PCA anisotropy*) and maximum scattering direction (ψ_0) of CNC suspensions undergoing the combined effect of shear flow and US radiation forces (step 2), followed by US radiation alone (step 3). Three regimes associated to three level of shear rates applied with same constant US radiation ($P \cong 297$ kPa) were highlighted $C = 9.1$ wt%, 0.01 mol L^{-1} NaCl.

For a low shear rate $\dot{\gamma}_{yx}$ = 0.84 s^{-1}, ψ_0 stayed around 180°, which corresponds to a predominant effect of the US radiation that forces the CNC director along the vertical direction. This is confirmed by the *PCA anisotropy* level that reaches the same value of about 0.24 in both steps 2 and 3. This was also the maximum value achieved for the three different shear-rates conditions explored. At intermediate shear rates level, $\dot{\gamma}_{yx}$ = 2.53 s^{-1}, at first the effect US radiation dominated the one due to shear ($\psi_0 \cong$180°) and then, at about t = 90 s, shear and US radiation started to acts together with nearly equivalent forces and the orientation of the CNC directors flipped towards nearly a "diagonal" orientation with ψ_0 values around 77° to 60° for a while. Consequently, applying the US radiation under shear at the beginning of step 2, seems to have firstly a predominant effect on shear flow forces, but after a while, unstable orientations, with ψ_0 between 90° and 180°, are observed. It highlights the competition between these two forces that would be at nearly equivalent strength at this specific shear rate of 2.53 s^{-1}. The associated *PCA anisotropy* followed this trend and was maximum when the US radiation dominates, but reached a lower value around 0.1 in the "diagonal" orientation. At the higher shear rate explored, $\dot{\gamma}_{yx}$ = 5.06 s^{-1}, the same scenario came at the beginning of step 2, but rapidly the effect of shear dominated the one of US radiation and ψ_0 is stabilized at around 80° to 90°. This corresponds to a mean orientation of the CNC director along the horizontal *y*-direction, but with a slightly larger distribution of orientations than in the step 1 (corresponding to shear flow alone). Independent of shear rate value, upon cessation of shear flow in step 3, US irradiation alone quickly moved ψ_0 to 180°. Nevertheless, one can see that for the highest preceding shear rates 5.06 s^{-1}, the time dependency of *PCA anisotropy* in step 3 was affected, and a longer time range was necessary to recover a higher value towards an equilibrium at ≅0.20. This value is indeed lower than the one of 0.24 reached for the lowest shear rate 0.84 s^{-1}, where US radiation continuously dominates.

All these features were also confirmed for a lower CNC concentration of C = 7.3 wt%, where the combined effect of shear flow and US led to some hesitation of the orientation at low shear rates $\dot{\gamma}_{yx}$ = 0.84 s^{-1} and 2.53 s^{-1} (Figures 6 a) and (Figure 6b) respectively and a dominating effect of shear over US radiation at a higher shear rate $\dot{\gamma}_{yx}$ = 8.45 s^{-1} (Figure 6c). These effects of ultrasound radiation and/or shear flow for CNC concentration C = 7.3 wt% were then observable with a very low content of cholesteric domains (tactoids at about ϕ_{LC} = 5 vol%). This hints at the possibility that the cholesteric domains of these CNC suspensions give no significant contribution to the orientation phenomena induced by US or shear flow. This idea is reinforced by the fact that under shear flow it has been shown that, above $\dot{\gamma}_{yx}$ = ~ 10 s^{-1} for C = 9 wt% (defined as the critical shear rate between regime II and regime III of the tree-regime flow curve), [44] the tactoids are completely disrupted and the structural organization of the suspension is likely a nematic liquid-crystal. Consequently, the orientation phenomena observed under US or shear flow could be principally associated to a global orientation of the CNCs organized in a nematic-like arrangement.

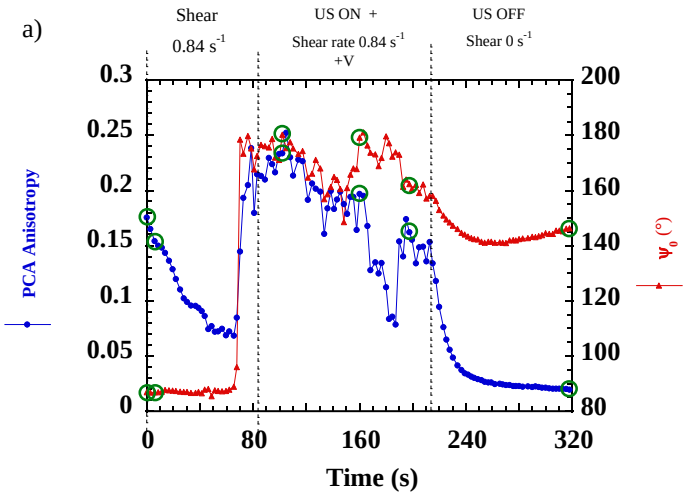

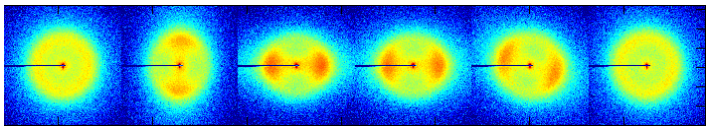

0 s 6 s 102 s 160 s 197 s 318 s

b)

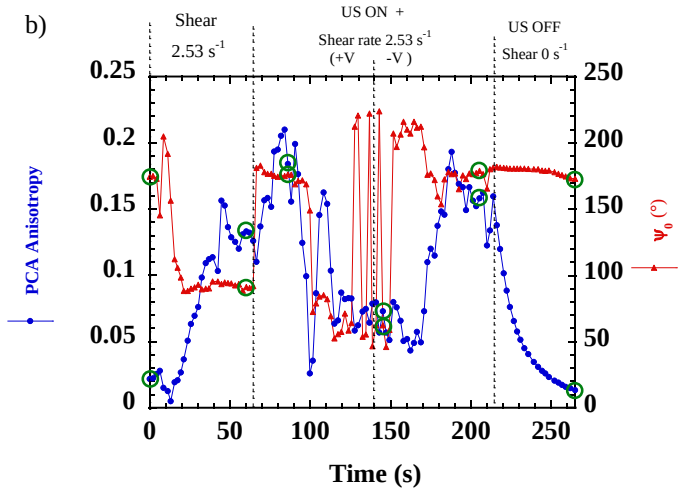

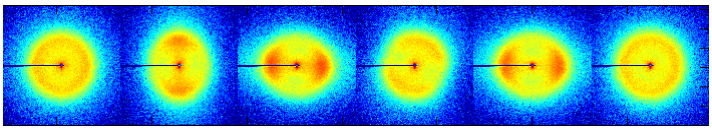

0 s 60 s 86 s 145 s 205 s 264 s

c)

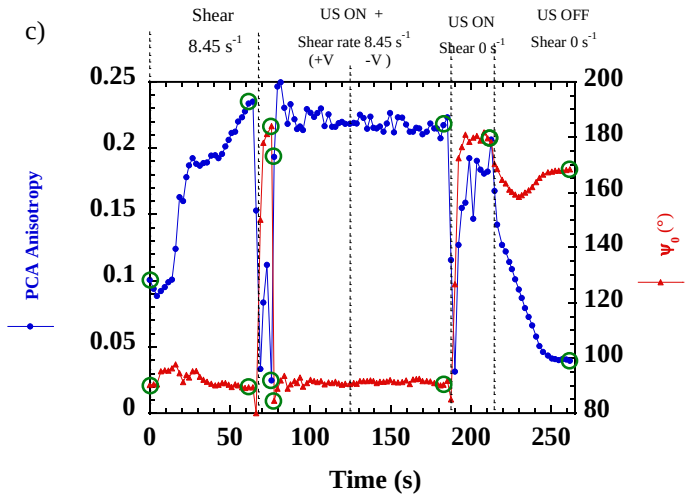

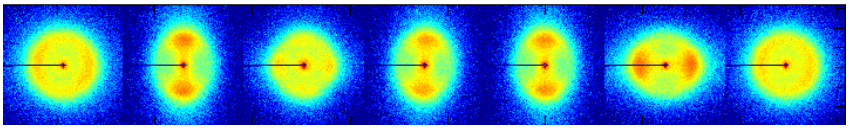

0 s 61 s 76 s 77 s 183 s 210 s 261 s

Figure 6: Transient state of orientation level (*PCA anisotropy*) and maximum scattering direction (ψ_0), and corresponding 2D-SAXS patterns of CNCs suspensions successively undergoing step 1: shear flow alone; setp2: shear flow along two successive velocity directions (+V) and (-V) associated to US radiation; step 3: US radiation alone; and step 4: shear flow and US radiation stopped. The applied shear rate was a) $\dot{\gamma}_{yx}$ = 0.84 s^{-1}, b) $\dot{\gamma}_{yx}$ = 2.53 s^{-1} and c) $\dot{\gamma}_{yx}$ = 8.45 s^{-1} and the acoustic pressure was $P \cong 297$ kPa. C = 7.3 wt%, 0.01 mol L^{-1} NaCl.

Two others parameters to take into account in the ability of US or shear flow to orient the nanocrystals are firstly the interparticle distance, *d,* between the nanocrystals, and secondly their mutual interactions. Doi and Edwards[68] have defined the boundary between dilute, semi-dilute, and concentrated domains, and have established the relationships between the volume fraction domain and the ability of rod-like particles with diameter D and length L to rotate under external forces. In the dilute domain, $\phi < (D/L)^2$, the average space available for each fiber is sufficient for it to freely rotate. In the semi-dilute domain, $(D/L)^2 < \phi < (D/L)$, the average space available for each fiber is only sufficient for it to rotate in a single plane. In the concentrated domain, $\phi > (D/L)$, the fiber rotation is severely restricted. The CNCs used in this study have $L \approx 120$ nm and $D \approx 20$ nm, and the theoretical approximated limits correspond to $(D/L)^2 \approx 2.8$ vol% and $(D/L) \approx 16.7$ vol%. Therefore, the two concentrations C = 7.3 wt% (ϕ = 4.69 vol%) and C = 9.1 wt% (ϕ = 5.88 vol%) for which the US radiation and shear flow have a clear effect on orientation of the CNCs were in the middle of the semi-dilute domain and correspond to situations with d = 34 nm and 30 nm, respectively. In addition, the lowest, studied concentration C = 5.2 wt% (ϕ = 3.31 vol%) was near the limit of the dilute to semi-dilute domain, with an interparticle distance

between CNCs around 40 nm. At this low concentration belonging to the isotropic domain (ϕ_{LC} = 0 wt%), no orientation under neither US radiation nor shear flow was detected (Figure S6). These features support the idea that the capacity of US radiation and shear flow to orientate CNCs is effective in a concentration domain for which the nanocrystals have reduced interparticle distance, i.e. with a reduced available space that enables the fibers to rotate only in a single plane. On the contrary, at lower concentration, with a larger interparticle distance allowing a larger freedom for the rotation of the nanorods, the power of these external forces is insufficient to induce measurable orientations in the range of the US power and shear rate explored in this work.

Comparison of relative levels of PCA anisotropy induced by shear or ultrasound. All the *PCA anisotropy* values that were achieved in steady state for sequentially increased shear flow levels are summarized in Figure 7. For the sake of comparison, the *PCA anisotropy* levels corresponding to combined shear flow and US were also plotted, using the values in the transient state when the US dominate the shear flow. The aim here is to compare the relative effect of these two solicitations on the measured *PCA anisotropy*, when the orientation induced by one of them clearly dominates the other. The results obtained at the two concentrations of C = 7.3 wt% and 9.1 wt % are also compared. For shear flow alone, the same procedure of successive shear rates applied in the two velocity directions were recorded, and the anisotropy values at increasing shear rates reported in Figure 7 correspond to the mean of the *PCA anisotropy* measured in both directions. Corresponding 2D-SAXS patterns of CNC suspensions undergoing horizontal shear flow alone and under simultaneous shear flow and US, were presented in Figure 7b and Figure 7c respectively. Some examples of time dependent evolutions under shear flow at several shear rates are presented in Figures S4, S5 and 6. The first outcome presented in Figure 7a revealed

PCA anisotropy levels that regularly increased as a function of shear rate as already observed in several previous works.[9,10,36-41-44,56] It seems to present a threshold in shear rate, at about 0.5 s^{-1}, below which the system is isotropic, and asymptotically tends towards a value of about 0.35. The second result was that under the simultaneous effect of shear flow and US radiation (when the equilibrium orientation is dominated by US), the *PCA anisotropy* is always higher at higher CNC concentrations. As suggested in the previous section, this would logically come from a better orientation of more concentrated CNC suspensions possessing lower interparticle distances. This would allow a better collective effect on the orientation of the liquid-crystal-like CNC suspensions induced by the US radiation forces.

Furthermore, the comparison between shear flow alone and combined shear flow and US effect highlighted a critical shear rate $\dot{\gamma}_c$ separating two situations in terms of *PCA anisotropy* levels. For $\dot{\gamma}_{yx} < \dot{\gamma}_c$, the *PCA anisotropy* of shear flow alone is lower than the case of simultaneous solicitations with US, and this corresponds to $\psi_0 \cong 180°$. On the contrary, for $\dot{\gamma}_{yx} > \dot{\gamma}_c$ the *PCA anisotropy* of shear flow alone is higher than the case of both simultaneous solicitations, and this corresponds to $\psi_0 \cong 90°$. This threshold is about $\dot{\gamma}_c \approx 15$ s^{-1} at $C = 9.1$ wt% (Figure 7a), while at $C = 7.3$ wt% it is at least $\dot{\gamma}_c \approx 8.45$ s^{-1} for which it has been shown that shear flow dominates the US radiation effect (Figure 6c). Consequently, at constant US irradiation, the critical shear rate $\dot{\gamma}_c$ needed to overcome the US radiation effect is higher at higher CNCs concentrations. This trend seems directly linked to the fact that, for a fixed US radiation, the US-induced orientation effect is higher at higher concentrations. Therefore, the suspension necessitates higher shear flow to succeed to flip the CNC director orientations towards the *y* horizontal direction of flow velocity.

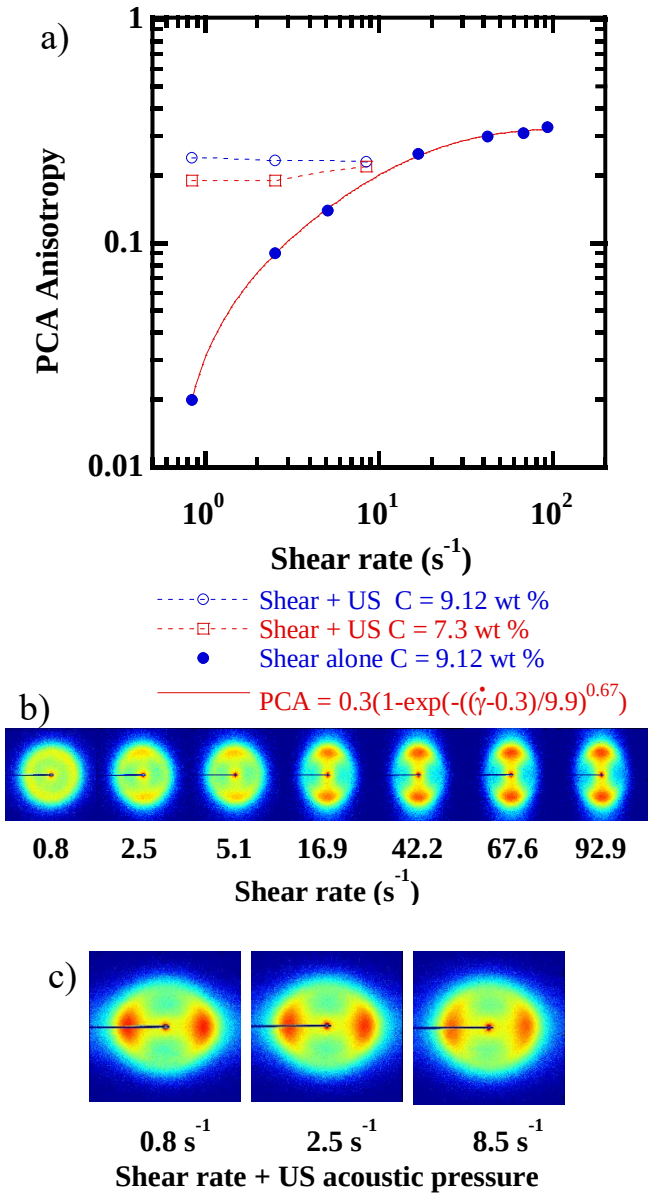

Figure 7. a) steady state of levels of orientation (*PCA anisotropy*) and b-c) corresponding 2D-SAXS patterns of CNC **suspensions undergoing horizontal shear flow alone [(b) and closed symbols in (a)], compared to measurements under simultaneous shear flow and US acoustic pressure $P \cong 297$ kPa [(c) and open symbols in (a)]. $C = 7.3$ wt% and 9.1 wt%, 0.01 mol L^{-1} NaCl.**

Concerning the pronounced effect of US radiation on the induced orientation of these CNCs' liquid crystals, one could ask the question of its physical origin.[5] This question has been addressed by several authors in the past, for higher frequency solicitations in the MHz domain and on smaller molecular length scales.[1-6,69-75] These theoretical and experimental studies were namely focused on the well-known acousto-optic effect, for the development of applications in underwater imaging and medical diagnostics. From these previous works, two main mechanisms have been proposed and summarized by Kozhevnikov[71] and more recently by Vitoriano[75]. The first mechanism of molecular orientation is a consequence of acoustical streaming arising from convective stresses; a high intensity sound wave can set up a flow pattern within a liquid-crystal cell, and this shear-flow pattern can realign the liquid-crystal director.[4,5,71-73] The second mechanism is of elastic nature and linked to the anisotropy of sound absorption by liquid crystals, which, according to Prigozhin's principle, must lead to the alignment of long nematic molecules in the direction of acoustic wave propagation.[2,70,74-75] Nevertheless, all these previous works have been focused on the high frequency range, typically above MHz, and the experimental evidenced have been performed at low length scales, and concern liquid crystals made of molecules or macromolecules, having rather small length scale. On the contrary, in the present study the orientation was obtained at 20 kHz, a much lower frequency range and at higher length scales corresponding to the nanometer (colloidal) sizes of the CNC liquid crystals studied. It was shown that the time scale involved to reach the US-induced stable nematic organization of CNCs is of the order of a few seconds, and the relaxation times after cessation of US to recover an equilibrium at low PCA anisotropy close to the isotropic value, is of the order of few minutes. Furthermore, this time-dependent increase or decrease of PCA anisotropy followed stretched exponential behaviors that can be associated to complex structural evolutions

involving several mechanisms. These features may suggest that the orientation due to the US in this frequency and for these colloidal objects is more likely to be associated to a streaming phenomenon (e.g. involving a time-dependent stabilization of flow) rather than a quicker elastic phenomenon induced by the anisotropy of sound absorption. Nevertheless, to be able to conclude on the relevant mechanism, some deeper investigations seemed to be necessary, as for example in situ velocity field determination inside the Shear flow/US-Cell by particle image velocimetry.[53]

CONCLUSIONS. The combined effect of two perpendicular forces, horizontal stress force induced by shear flow and vertical acoustic radiation force induced by ultrasound waves, on the dynamical structural orientations of liquid-crystal-like CNC suspensions, were studied by time-resolved in situ SAXS in dedicated channel type shear flow/ultrasound cells. The time dependent evolutions of the 2D-SAXS patterns were analyzed by model-free Principal Component Analysis, and allowed to describe accurately both the level of orientation and the direction of alignment of the CNC director, according to the different applied solicitations.

It has been shown that US radiation can be used to control the alignment of liquid crystal organization of CNC suspensions with their director aligned along the vertical ultrasonic wave propagation direction. Confirming that the application of shear flow induces the orientation of CNC directors along the horizontal velocity direction, it was finally shown that tuning the intensities of these two perpendicular solicitations applied simultaneously allows the control over the equilibrium orientation (or out of equilibrium orientation, “hesitations”) directions of the CNC director. For a constant applied US radiation, at increasing shear rates three regimes were observed. At low shear rate, a predominant effect of the US radiation is observed, causing an

equilibrium orientation of the CNC director along the vertical direction. At intermediate shear rates, an out of equilibrium "hesitation" orientation is observed with sometimes intermediate “diagonal” orientations that are reached for a while. At high shear rate, the shear flow dominate over the US radiation, corresponding to an equilibrium orientation of the CNC director along the horizontal flow direction.

Furthermore, the comparison between shear flow effect alone and combined shear flow and US effects, enabled to highlight a critical shear rate $\dot{\gamma}_c$ separating two situations. Below $\dot{\gamma}_c$ the *PCA anisotropy* is higher for the combine effect of US and shear flow, in contrast above $\dot{\gamma}_c$ the shear flow alone give rise to a higher level of orientation.

ASSOCIATED CONTENT

Supporting Information.

The Supporting Information is available free of charge on the ACS Publications website. Scattering intensity, anisotropic phase transition and CNC interparticle distance as a function of CNC concentration, calculation of different shear rates in the channel as a function of different shear flow regimes, transient state of *PCA anisotropy*, ψ_0 and corresponding 2D-SAXS patterns of CNC's suspensions submitted to shear flow and/or US radiation, at different concentrations.

AUTHOR INFORMATION

Corresponding Author

*Frédéric Pignon. frederic.pignon@univ-grenoble-alpes.fr , Univ. Grenoble Alpes, CNRS, Grenoble INP (Institute of Engineering Univ. Grenoble Alpes), LRP, F-38000 Grenoble

Authors Contributions

Frédéric Pignon: Conceptualization, Methodology, Writing- Original, draft preparation, Writing- Reviewing and Editing, Investigation, Formal analysis. E. F. Semeraro: Software, Formal analysis, Writing- Reviewing and Editing., W.Chèvremont, H. Bodiguel, N. Hengl, M. Sztucki: Investigation, Formal analysis, Writing- Reviewing and Editing, M. Karrouch: Investigation.

Notes

The authors declare no competing financial interest.

ACKNOWLEDGMENT

We thank Jacques Gorini (ESRF, Grenoble), Didier Blésès, Frédéric Hugenell and Eric Faivre (Laboratoire Rhéologie et Procédés) for technical assistance. ESRF is acknowledged for support during synchrotron beamtime (IN-1071). LRP is part of Institut Carnot PolyNat (Investissements d'Avenir - grant agreement #ANR-16-CARN-0025-01), LabEx Tec21 (Investissements d'Avenir - grant agreement no. ANR-11-LABX-0030) and Glyco@Alps programme (Investissements d'Avenir - grant agreement #ANR-15-IDEX-02).

ABBREVIATIONS

US, ultrasound, SAXS, small angle x-ray scattering, SALS, small-angle light scattering, CNC, cellulose nanocrystal, ESRF, European synchrotron radiation facility, PCA, principal component analysis.

REFERENCES

(1) Helfrich, W. Orienting action of sound on nematic liquid crystals. *Phys. Rev. Lett.* **1972**, *29(24)*, 1583–1586.

(2) Biscari, P.; DiCarlo, A.; Turzi, S.S. Anisotropic wave propagation in nematic liquid crystals. *Soft Matter* **2014**, *10*, 8296

(3) Mailer, H.; Likins, K. L.; Taylor, T. R.; Fergason, J. L. Effect of ultrasound on a nematic liquid crystal. *Appl. Phys. Lett.* **1971,** *18(4)*, 105–107.

(4) Nagaï S.; Peters A.; Candau S. Acousto-optical effects in a nematic liquid crystal. R*ev. Phys. Appl. (Paris)* **1977**, *12*, 21-30.

(5) Kapustina O.A. On the mechanism of the effect of ultrasound on a nematic liquid crystal at oblique incidence. *Acoustical Physics*, **2008**, *54(6)*, 778-782.

(6) Harada, Y.; Koyama, D.; Fukui, M.; Emoto, A.; Nakamura L.; Matsukawa, M. Molecular orientation in a variable-focus liquid crystal lens induced by ultrasound vibration. *Sci. Rep*. **2020**, *10*, 6168.

(7) Revol, J.-F.; Bradford, H.; Giasson, J.; Marchessault, R.H.; Gray D.G. Helicoidal self-ordering of cellulose microfibrils in aqueous suspension. *Int. J. Biol. Macromol.* **1992**, *14*, 170–172.

(8) Dong, X.M.; Kimura, T.; Revol, J.-F.; Gray, D.G. Effects of ionic strength on the isotropic−chiral nematic phase transition of suspensions of cellulose crystallites. *Langmuir* **1996**, *12*, 2076–2082.

(9) Orts, W.J.; Godbout, L.; Marchessault, R.H.; Revol, J.-F. Enhanced ordering of liquid crystalline suspensions of cellulose microfibrils: A small angle neutron scattering study. *Macromolecules* **1998**, *31*, 5717–5725.

(10) Ebeling, T.; Paillet, M.; Borsali, R.; Diat, O.; Dufresne, A.; Cavaillé, J.-Y.; Chanzy, H. Shear-induced orientation phenomena in suspensions of cellulose microcrystals, revealed by small angle X-ray scattering. *Langmuir* **1999**, *15*, 6123–6126.

(11) Ureña-Benavides, E.E.; Ao, G.; Davis, V.A.; Kitchens, C.L. Rheology and phase behavior of lyotropic cellulose nanocrystal suspensions. *Macromolecules* **2011**, *44*, 8990–8998.

(12) Lagerwall, J.P.F.; Schütz, C.; Salajkova, M.; Noh, J.; Park, J.H.; Scalia, G.; Bergstrom, L. Cellulose nanocrystal-based materials: from liquid crystal self-assembly and glass formation to multifunctional thin films. *Npg Asia Materials* **2014**, *6*, e80.

(13) Schütz, C.; Agthe, M.; Fall, A. B.; Gordeyeva, K.; Guccini, V.; Salajková, M.; Plivelic, T. S.; Lagerwall, J. P. F.; Salazar-Alvarez, G.; Bergström, L. Rod packing in chiral nematic cellulose nanocrystal dispersions studied by small-angle X-ray scattering and laser diffraction. *Langmuir* **2015**, *31*, 6507–6513.

(14) Lenfant, G.; Heuzey, M.-C.; van de Ven, T.G.M.; Carreau, P.J. A comparative study of ECNC and CNC suspensions: effect of salt on rheological properties. *Rheol. Acta* **2017**, *56*, 51–62.

(15) Gicquel, E.; Bras, J.; Rey, C.; Putaux, J.-L.; Pignon, F.; Jean, B.; Martin, C. Impact of sonication on the rheological and colloidal properties of highly concentrated cellulose nanocrystal suspensions. *Cellulose* **2019**, *26*, 7619–7634.

(16) Xu, Y.; Atrens, A.; Stokes, J.R. A review of nanocrystalline cellulose suspensions: Rheology, liquid crystal ordering and colloidal phase behaviour. *Adv. Colloid Interface Sci.* **2020**, 275, 102076.

(17) Wang, P.; Hamad, W.; MacLachlan, M. Structure and transformation of tactoids in cellulose nanocrystal suspensions. *Nat. Commun*. **2016**, *7*, 11515.

(18) Wang, P.-X.; MacLachlan, M.J. Liquid crystalline tactoids: ordered structure, defective coalescence and evolution in confined geometries. *Phil. Trans. R. Soc. A* **2018**, *376*, 20170042.

(19) Tran, A.; Hamad, W.Y.; MacLachlan, M.J. Fabrication of cellulose nanocrystal films through differential evaporation for patterned coatings. *ACS Appl. Nano Mater.* **2018**, *1*, 3098−3104.

(20) Tran, A.; Hamad, W.Y.; MacLachlan, M.J. Tactoid Annealing improves order in self-assembled cellulose nanocrystal films with chiral nematic structures. *Langmuir* **2018,** *34* (2), 646-652.

(21) Liu, Y.; Schütz, C.; Salazar-Alvarez, G.; Bergström, L. Assembly, gelation, and helicoidal consolidation of nanocellulose dispersions. *Langmuir* **2019**, *35*, 3600–3606.

(22) Schütz, C.; Bruckner, J.R.; Honorato-Rios, C.; Tosheva, Z.; Anyfantakis, M.; Lagerwall, J.P.F. From Equilibrium Liquid Crystal Formation and Kinetic Arrest to Photonic Bandgap Films Using Suspensions of Cellulose Nanocrystals. *Crystals* **2020**, 10, 199.

(23) Mitov, M. Chlolesteric liquid crystals in living matter. *Soft Matter* **2017**, *13*, 4176–4209.

(24) Siqueira, G.; Bras, J.; Dufresne, A. Cellulosic bionanocomposites: A review of preparation, properties and applications. *Polymers* **2010**, *2*, 728–765.

(25) Dufresne, A. Nanocellulose: From Nature to High Performance Tailored Materials, 2nd ed.; Walter de Gruyter GmbH: Berlin/Boston, **2017**.

(26) Tang A.; Li, J.; Li, J.; Zhao, S.; Liu, W.; Liu, T.; Wang, J.; Liu, Y. A. Nanocellulose/PEGDA aerogel scaffolds with tunable modulus prepared by stereolithography for three-dimensional cell culture. *Biomater. Sci. Polym.* **2019**, *30*, 797–814.

(27) Thomas, B.; Raj, M.C.; Athira, K.B.; Rubiyah, M.H; Joy, J.; Moores, A.; Drisko, G.L.; Sanchez, C. Nanocellulose, a versatile green platform: from biosources to materials and their applications. *Chem. Rev.* **2018**, *118*, 11575−11625.

(28) De France K.J.; Zeng, Z.; Wu, T.; Nyström, G. Functional Materials from Nanocellulose: Utilizing Structure–Property Relationships in Bottom-Up Fabrication. *Adv. Mater.* 2020, 2000657.

(29) Frka-Petesic, B.; Radavidson, H.; Jean, B.; Heux, L. Dynamically controlled iridescence of cholesteric cellulose nanocrystal suspensions using electric fields. *Adv. Mater.* **2017**, *29*, 1606208.

(30) Domingues, R.M.A.; Gomes, M.E.; Rei, R.L. The potential of cellulose nanocrystals in tissue engineering strategies. *Biomacromolecules* **2014**, *15*, 2327–2346.

(31) Kargarzadeh, H.; Huang, J.; Lin, N.; Ahmad, I.; Mariano, M.; Dufresne, A.; Thomas, S.; Gałęski, A. Recent developments in nanocellulose-based biodegradable polymers, thermoplastic polymers, and porous nanocomposites. *Prog. Polym. Sci.* **2018**, *87*, 197−227.

(32) Azzam, F.; Heux, L.; Putaux, J.-L.; Jean, B. Preparation by grafting onto, characterization, and properties of thermally responsive polymer-decorated cellulose nanocrystals. *Biomacromolecules* **2010**, *11*, 3652-3659.

(33) Azzam, F.; Siaueira, E.; Fort, S.; Hassaini, R.; Pignon, F.; Travelet, C.; Putaux, J. -L.; Jean, B. Tunable aggregation and gelation of thermoresponsive suspensions of polymer-grafted cellulose nanocrystals. *Biomacromolecules* **2016**, *17*, 2112-2119.

(34) Gicquel, E.; Martin, C.; Heux, L.; Jean, B.; Bras, J. Adsorption versus grafting of poly(N-Isopropylacrylamide) in aqueous conditions on the surface of cellulose nanocrystals. *Carbohydr. Polym.* **2019**, *210*, 100-109.

(35) Lin, F., Pignon, F. Putaux, J.L. and Jean B. Temperature-triggered formation of a cellulose II nanocrystal network through regioselective derivatization. *Nanoscale* **2021***, 13,* 6447-6460.

(36) Bercea, M.; Navard, P. Shear dynamics of aqueous suspensions of cellulose whiskers. *Macromolecules* **2000**, *33*, 6011–6016.

(37) Shafiei-Sabet, S.; Hamad, W.Y.; Hatzikiriakos, S.G. Rheology of nanocrystalline cellulose aqueous suspensions. *Langmuir* **2012**, *28*, 17124–17133.

(38) Shafiei-Sabet, S.; Hamad, W.Y.; Hatzikiriakos, S.G. Ionic strength effects on the microstructure and shear rheology of cellulose nanocrystal suspensions. *Cellulose* **2014**, *21*, 3347–3359.

(39) Derakhshandeh, B.; Petekidis, G.; Shafiei-Sabet, S.; Hamad, W.Y.; Hatzikiriakos, S.G. Ageing, yielding, and rheology of nanocrystalline cellulose suspensions. *J. Rheol.* **2013**, *57*, 131–148.

(40) Haywood, A.D.; Weigandt, K.M.; Saha, P.; Noor, M.; Green, M.J.; Davis V.A. New insights into the flow and microstructural relaxation behavior of biphasic cellulose nanocrystal dispersions from RheoSANS. *Soft Matter* **2017**, *13*, 8451–8462.

(41) Xu, Y.; Atrens, A.D.; Stokes, J.R. Rheology and microstructure of aqueous suspensions of nanocrystalline cellulose rods. *J. Colloid Interface Sci.* **2017**, *496*, 130–140.

(42) Sanchez-Botero, L.; Dimov, A.V.; Li, R.; Smilgies, D.-M.; Hinestroza, J.O. In situ and real-time studies, via synchrotron X-ray scattering, of the orientational order of cellulose nanocrystals during solution shearing. *Langmuir* **2018**, *34*, 5263−5272

(43) Qi, W.; Yu, J.; Zhang, Z.; Xu, H-N. Effect of pH on the aggregation behavior of cellulose nanocrystals in aqueous medium. *Mater. Res. Express* **2019**, *6*, 125078.

(44) Pignon, F.; Challamel, M.; De Geyer, A.; Elchamaa, M.; Semeraro, E.F.; Hengl, N.; Jean, B.; Putaux, J.L.; Gicquel, E.; Bras, J., et al. Breakdown and buildup mechanisms of cellulose nanocrystal suspensions under shear and upon relaxation probed by SAXS and SALS. *Carbohydr. Polym.* **2021**, *260*, 117751.

(45) Sugiyama,J.; Chanzy, H.; Maret, G. Orientation of cellulose microcrystals by strong magnetic fields. *Macromolecules* **1992**, *25*, 4232.

(46) Frka-Petesic, B.; Sugiyama, J.; Kimura, S.; Chanzy, H. ; Maret, G. Negative Diamagnetic Anisotropy and Birefringence of Cellulose Nanocrystals. *Macromolecules* **2015**, *48*, 8844.

(47) De France, K. J.; Yager, K. G.; Hoare,T.; Cranston, E. D. Cooperative Ordering and Kinetics of Cellulose Nanocrystal Alignment in a Magnetic Field. *Langmuir* **2016**, *32*, 7564.

(48) Parker, R.M.; Frka-Petesic,B.; Guidetti,G.; Kamita,G.; Consani, G.; Abell, C.; Vignolini. S. Hierarchical Self-Assembly of Cellulose Nanocrystals in a Confined Geometry. *ACS Nano* **2016**, *10 (9)*, 8443-8449.

(49) Chen T.; Zhao, Q.; Meng, X.; Li, Y.; Peng, H.; Whittaker, A.K.; Zhu. S. Ultrasensitive Magnetic Tuning of Optical Properties of Films of Cholesteric Cellulose Nanocrystals. *ACS Nano* **2020**, *14 (8)*, 9440-9448.

(50) Cherpak, V.; Korolovych V. F.; Geryak R.; Turiv T.; Nepal D.; Kelly J.; Bunning T.J.; Lavrentovich O. D.; Heller W. T.; Tsukruk V. V. Robust Chiral Organization of Cellulose Nanocrystals in Capillary Confinement. *Nano Lett.* **2018**, *18(11)*, 6770–6777.

(51) Gray, D.G.; Mu, X. Twist–bend stage in the relaxation of sheared chiral nematic suspensions of cellulose nanocrystals. *ACS Omega* **2016**, *1*, 212–219.

(52) Jin, Y.; Hengl, N.; Baup, S.; Pignon, F.; Gondrexon, N.; Sztucki, M.; Romdhane, A.; Guillet, A.; Aurousseau, M. Ultrasonic assisted cross-flow ultrafiltration of starch and cellulose nanocrystals suspensions: Characterization at multi-scales. *Carbohydr. Polym.* **2015**, *124*, 66–76.

(53) Rey, C.; Hengl, N.; Baup, S.; Karrouch, M.; Gicquel, E.; Dufresne, A.; Djeridi, H.; Dattani, R.; Jin, Y.; Pignon, F. Structure, rheological behavior and in situ local flow-fields of cellulose nanocrystal dispersions during cross-flow ultrafiltration. *ACS Sustain. Chem. Eng.* **2019**, *7*, 10679−10689.

(54) Semeraro, E.F.; Hengl, N.; Karrouch, M;, Michot, L.J.; Paineau, E.; Jean, B.; Putaux, J.-L.; Lancelon-Pin, C.; Sharpnack, L.; Pignon, F. Layered organization of anisometric cellulose nanocrystals and beidellite clay particles accumulated near the membrane surface during cross-flow ultrafiltration: In situ SAXS and ex situ SEM/WAXD characterization. *Colloids Sur. A* **2020**, *584*, 124030.

(55) Rosén, T.; Wang, R.; Zhan C.; He, H.; Chodankar, S.; Benjamin, S.; Hsiao, B.S. Cellulose nanofibrils and nanocrystals in confined flow: Single-particle dynamics to collective alignment revealed through scanning small-angle x-ray scattering and numerical simulations. *Phys. Rev. E* **2020**, *101*, 032610.

(56) Kádár, R.; Stefan Spirk, S.; Nypelö, T. Cellulose Nanocrystal Liquid Crystal Phases: Progress and Challenges in Characterization Using Rheology Coupled to Optics, Scattering, and Spectroscopy. *ACS Nano* **2021**, *15*, 7931–7945.

(57) Bardet, R.; Belgacem, N.; Bras, J. Flexibility and color monitoring of cellulose nanocrystal iridescent solid films using anionic or neutral polymers. *ACS Appl. Mater. Interfaces* **2015**, *7 (7)*, 4010-4018.

(58) Schwartz, M.; Lenzini, G.; Geng, Y., Rønne, P. B.; Ryan, P. Y. A.; Lagerwall, J. P. F. Cholesteric liquid crystal shells as enabling material for information-rich design and architecture. *Adv. Mater.* **2018**, *30*, 1707382.

(59) Hausmann, M.K.; Rühs, P.A.; Siqueira, G.; Läuger, J.; Libanori, R.; Zimmermann, T.; Studart. A.R. Dynamics of Cellulose Nanocrystal Alignment during 3D Printing. *ACS Nano* **2018**, *12 (7)*, 6926-6937.

(60) Kose, O.; Tran, A.; Lewis, L.; Hamad, W.Y.; MacLachlan, M.J. Unwinding a spiral of cellulose nanocrystals for stimuli-responsive stretchable optics. *Nat. Commun*. **2019**, *10*, 510.

(61) Zhang, R.; Chu,G.; Vasilyev, G.; Martin, P.; Camposeo, A.; Persano, L.; Pisignano, D.; Zussman; E. Hybrid Nanocomposites for 3D Optics: Using Interpolymer Complexes with Cellulose Nanocrystals. *ACS Appl. Mater. Interfaces* **2019,** *11 (21)*, 19324-19330.

(62) Zhang, X.; Xiong, R.; Kang, S.; Yang, Y.; Tsukruk. V.V. Alternating Stacking of Nanocrystals and Nanofibers into Ultrastrong Chiral Biocomposite Laminates. *ACS Nano* **2020**, *14 (11)*, 14675-14685.

(63) Shimizu, Y.; Koyama,D.; Fukui, M.; Akira Emoto, A.; Nakamura, K.; Matsukawa M. Ultrasound liquid crystal lens. *Appl. Phys. Lett.* **2018**, *112*, 161104.

(64) Gibaud, T.; Dagès, N.; Lidon, P.; Jung, G.; Ahouré, L.C.; Sztucki, M.; Poulesquen, A.; Hengl, N.; Pignon, F.; Manneville, S. Rheoacoustic gels: tuning mechanical and flow properties of colloidal gels with ultrasonic vibrations. *Phys. Rev. X* **2020**, *10*, 011028.

(65) Narayanan, T.; Sztucki, M.; Van Vaerenbergh, P.; Léonardon, J.; Gorini, J.; Claustre, L.; Sever, F.; Morse, J.; Boesecke, P. A multipurpose instrument for time-resolved ultra-small-angle and coherent X-ray scattering. *J. Appl. Crystal.* **2018**, *51*, 1–14.

(66) Muthig, M.; Prévost, S.; Orglmeister, R.; Gradzielski, M. SASET: A program for series analysis of small-angle scattering data. *J. Appl. Crystal.* **2013**, *46*, 1187–1195.

(67) Son, Y. Determination of shear viscosity and shear rate from pressure drop, and flow rate relationship in a rectangular channel. *Polymer* **2007**, *48*, 632–637.

(68) Doi M, Edwards, SF (1986) The theory of polymer dynamics. Clarendon, Oxford

(69) Kapustina O. A. Ultrasound-Initiated Structural Transformations in Liquid Crystals (A Review). *Acoust. Phys.* **2008**, *54(2)*, 180-196.

(70) Selinger, J.V.; Spector, M.S.; Greanya,V.A.; Weslowski, B.T.; Shenoy, D.K.; Shashidhar, R. Acoustic realignment of nematic liquid crystals. *Phys. Rev. E* **2002**, *66*, 051708.

(71) Kozhevnikov, E.N. Deformation of a homeotropic nematic liquid crystal layer at oblique incidence of an ultrasonic wave. *Acoust. Phys.* **2005**, *51*, 688-694.

(72) Kozhevnikov, E.N. Acoustic Streaming in a Nematic Liquid Crystal Layer under Binary Action of Sound Waves and Viscous Waves Acoustical Physics. *Acoust. Phys.* **2010**, *56*, 24-32.

(73) Toda, K.; Inoue, M.; Moritake, H.; Yoshino, K. Analysis of acoustic streaming in nematic liquid-crystal cell. *Jpn. J. Appl. Phys.* **2005**, *44,* 316-323.

(74) Dion J.L.; Jacob A.D. A new hypothesis on ultrasonic interaction with a nematic liquid crystal. *J. Appl. Phys.* **1977**, *31(8)*, 490-493.

(75) Vitoriano C. Acousto-optic effect in nematic liquid crystals: Experimental evidence of an elastic regime. *Phys. Rev. E* **2013**, *88*, 032501.

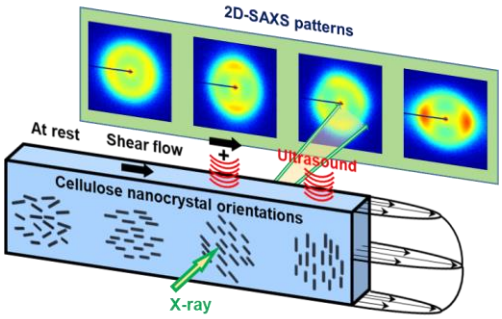

TOC Graphic